In Vitro Extension and Phosphorylation of CasSD

NC-biotinylated or C-biotinylated CasSD bound to avidin-coated latex membrane was prepared as described above. After stretching of latex membrane or without stretching, biotinylated CasSD proteins were washed three times with 0.25% Triton X-100 and 2% BSA in buffer A (20 mM HEPES [pH 7.5], 150 mM NaCl, 4 mM $MgCl_2$, 1 mM DTT, 1 mM PMSF, 20 μg/ml aprotinin, 0.5 mM EGTA) and three times with 0.1% BSA in buffer A and incubated with recombinant kinases (specific activity of each kinase used: 700 pmol/min phosphate transfer) in 350 μl of kinase reaction buffer (20 mM HEPES [pH 7.5], 0.9 mM ATP, 0.1% BSA, 140 mM NaCl, 10 mM $MgCl_2$, 3 mM $MnCl_2$, 0.5 mM EGTA, 20 μg/ml aprotinin, 1.5 mM DTT, 1.5 mM Na_3VO_4, 0.03% Brij-35) for 2 min at room temperature. After kinase reaction, biotinylated CasSD proteins were washed three times with ice-cold 1% Triton X-100 in PBS containing 1 mM Na_3VO_4, recovered, and solubilized by incubation with 1× SDS sample buffer containing 0.12 M DTT at 95°C for 5 min. Tyrosine phosphorylation of CasSD was determined by anti-phospho-Cas immunoblotting and avidin affinity blotting.

In Vitro Binding of αCas1 to Extended CasSD

NC-biotinylated or C-biotinylated CasSD bound to avidin-coated latex membrane was either extended (100%) or left unextended in PBS containing 1% Triton X-100, 2% BSA, 5% FBS, 1 mM DTT, 20 μg/ml aprotinin, and 0.5 mM EGTA. After 10 min, CasSD proteins on the latex surface were washed three times and incubated for 30 min with PBS containing 2% BSA, 5% FBS, 1 mM DTT, 20 μg/ml aprotinin, and 0.5 mM EGTA to block nonspecific binding and then incubated for 2 min with αCas1 diluted at 1:1200 in the same buffer. After six washes with PBS containing 0.1% Tween-20 and 1 mM DTT, bound proteins were solubilized with 1× SDS sample buffer containing 0.12 M DTT and subjected to SDS-PAGE followed by anti-rabbit IgG or αCas1 immunoblotting and avidin affinity blotting.

Binding of Two Different Anti-Cas Antibodies, αCas1 and αCas3, to Triton Cytoskeletons

Triton cytoskeletons were prepared from Cas-deficient fibroblasts transiently expressing RFP-Cas or RFP alone as described previously (Sawada and Sheetz, 2002). After two washes with buffer A containing 2% BSA and 5% FBS, the buffer was replaced with the buffer A containing 0.5 mM ATP, 2% BSA, 5% FBS, and either αCas1 or αCas3 (1:400 dilution), and Triton cytoskeletons were either stretched or left unstretched. After 2 min of incubation, samples were washed two times with buffer A containing 2% BSA and 5% FBS and four times with buffer A, solubilized with 1× SDS sample buffer containing 20 mM DTT, and subjected to SDS-PAGE followed by anti-rabbit IgG, αCas2, and anti-actin immunoblotting (Figure 5B, upper panel).

Immunofluorescence Staining, Fluorescence Microscopy, and Image Display

Twenty minutes after being plated on collagen (Type-I)-coated coverslips, Cas-deficient fibroblasts expressing RFP-Cas were washed with PBS; fixed with 3.7% formaldehyde in PBS; permeabilized with 0.1% Triton X-100 in PBS; stained using αCas1, αCas3, or pCas-165 as a primary antibody (1:400 dilution for αCas1 and αCas3 and 1:100 dilution for pCas-165) and Alexa Fluor 488 anti-rabbit IgG as a secondary antibody; and then viewed with a confocal microscope (Olympus IX-81 with FV500 system). Image intensity from the green channel (immunofluorescence with αCas1, αCas3, or pCas-165) and the red channel (RFP-Cas) was displayed with the contrast enhanced by setting the highest intensity in each image at the maximum value of the dynamic range and the background (cell-free area) at zero in ImageJ, a free open source Java imaging platform (http://rsb.info.nih.gov/ij/).

Statistical Analysis

Statistical analysis was performed with the paired Student's t test, and $p < 0.05$ was defined as significant.

Supplemental Data

The Supplemental Data include Supplemental Experimental Procedures and one supplemental figure and can be found with this article online at http://www.cell.com/cgi/content/full/127/5/1015/DC1/.

ACKNOWLEDGMENTS

We thank S. Ohkubo, T. Mandai, M. Cull, M. Galbmillion, and M.L. Bushey for assisting in the construction of the IPE system; P.S. Low, S.K. Hanks, T. Yamamoto, and M. Matsuda for the plasmids; J.M. Fernandez, M. Edidin, T.D. Perez, A. Sakakibara, C.D. Hu, H. Takayanagi, T. Miyazaki, T. Tezuka, M. Saitoh, K. Takeda, H. Ichijo, and K. Nakamura for helpful discussions and consistent support. This work was supported by NIH grant R01 EB001480.

Received: June 9, 2006
Revised: August 20, 2006
Accepted: September 25, 2006
Published: November 30, 2006

REFERENCES

Balaban, N.Q., Schwarz, U.S., Riveline, D., Goichberg, P., Tzur, G., Sabanay, I., Mahalu, D., Safran, S., Bershadsky, A., Addadi, L., and Geiger, B. (2001). Force and focal adhesion assembly: A close relationship studied using elastic micropatterned substrates. Nat. Cell Biol. *3*, 466–472.

Ballestrem, C., Erez, N., Kirchner, J., Kam, Z., Bershadsky, A., and Geiger, B. (2006). Molecular mapping of tyrosine-phosphorylated proteins in focal adhesions using fluorescence resonance energy transfer. J. Cell Sci. *119*, 866–875.

Bougeret, C., Rothhut, B., Jullien, P., Fischer, S., and Benarous, R. (1993). Recombinant Csk expressed in Escherichia coli is autophosphorylated on tyrosine residue(s). Oncogene *8*, 1241–1247.

Briknarova, K., Nasertorabi, F., Havert, M.L., Eggleston, E., Hoyt, D.W., Li, C., Olson, A.J., Vuori, K., and Ely, K.R. (2005). The serine-rich domain from Crk-associated substrate (p130Cas) is a four-helix bundle. J. Biol. Chem. *280*, 21908–21914.

Carrion-Vazquez, M., Oberhauser, A.F., Fowler, S.B., Marszalek, P.E., Broedel, S.E., Clarke, J., and Fernandez, J.M. (1999). Mechanical and chemical unfolding of a single protein: A comparison. Proc. Natl. Acad. Sci. USA *96*, 3694–3699.

Chen, H.C., Appeddu, P.A., Parsons, J.T., Hildebrand, J.D., Schaller, M.D., and Guan, J.L. (1995). Interaction of focal adhesion kinase with cytoskeletal protein talin. J. Biol. Chem. *270*, 16995–16999.

Chien, S., Li, S., Shiu, Y.T., and Li, Y.S. (2005). Molecular basis of mechanical modulation of endothelial cell migration. Front. Biosci. *10*, 1985–2000.

Cooper, J.A., Esch, F.S., Taylor, S.S., and Hunter, T. (1984). Phosphorylation sites in enolase and lactate dehydrogenase utilized by tyrosine protein kinases in vivo and in vitro. J. Biol. Chem. *259*, 7835–7841.

Defilippi, P., Di Stefano, P., and Cabodi, S. (2006). p130Cas: A versatile scaffold in signaling networks. Trends Cell Biol. *16*, 257–263.

Dubin-Thaler, B.J., Giannone, G., Dobereiner, H.G., and Sheetz, M.P. (2004). Nanometer analysis of cell spreading on matrix-coated surfaces reveals two distinct cell states and STEPs. Biophys. J. *86*, 1794–1806.

Fisher, T.E., Oberhauser, A.F., Carrion-Vazquez, M., Marszalek, P.E., and Fernandez, J.M. (1999). The study of protein mechanics with the atomic force microscope. Trends Biochem. Sci. *24*, 379–384.

Fonseca, P.M., Shin, N.Y., Brabek, J., Ryzhova, L., Wu, J., and Hanks, S.K. (2004). Regulation and localization of CAS substrate domain tyrosine phosphorylation. Cell. Signal. *16*, 621–629.

Geiger, B., and Bershadsky, A. (2002). Exploring the neighborhood: Adhesion-coupled cell mechanosensors. Cell *110*, 139–142.

Giannone, G., and Sheetz, M.P. (2006). Substrate rigidity and force define form through tyrosine phosphatase and kinase pathways. Trends Cell Biol. *16*, 213–223.

Giannone, G., Dubin-Thaler, B.J., Dobereiner, H.G., Kieffer, N., Bresnick, A.R., and Sheetz, M.P. (2004). Periodic lamellipodial contractions correlate with rearward actin waves. Cell *116*, 431–443.

Harte, M.T., Hildebrand, J.D., Burnham, M.R., Bouton, A.H., and Parsons, J.T. (1996). p130Cas, a substrate associated with v-Src and v-Crk, localizes to focal adhesions and binds to focal adhesion kinase. J. Biol. Chem. *271*, 13649–13655.

Hattori, M., and Minato, N. (2003). Rap1 GTPase: Functions, regulation, and malignancy. J. Biochem. (Tokyo) *134*, 479–484.

Hu, C.D., Chinenov, Y., and Kerppola, T.K. (2002). Visualization of interactions among bZIP and Rel family proteins in living cells using bimolecular fluorescence complementation. Mol. Cell *9*, 789–798.

Huang, J., Hamasaki, H., Nakamoto, T., Honda, H., Hirai, H., Saito, M., Takato, T., and Sakai, R. (2002). Differential regulation of cell migration, actin stress fiber organization, and cell transformation by functional domains of Crk-associated substrate. J. Biol. Chem. *277*, 27265–27272.

Isakov, N., Wange, R.L., Watts, J.D., Aebersold, R., and Samelson, L.E. (1996). Purification and characterization of human ZAP-70 protein-tyrosine kinase from a baculovirus expression system. J. Biol. Chem. *271*, 15753–15761.

Jiang, G., Giannone, G., Critchley, D.R., Fukumoto, E., and Sheetz, M.P. (2003). Two-piconewton slip bond between fibronectin and the cytoskeleton depends on talin. Nature *424*, 334–337.

Katsumi, A., Milanini, J., Kiosses, W.B., del Pozo, M.A., Kaunas, R., Chien, S., Hahn, K.M., and Schwartz, M.A. (2002). Effects of cell tension on the small GTPase Rac. J. Cell Biol. *158*, 153–164.

Klinghoffer, R.A., Sachsenmaier, C., Cooper, J.A., and Soriano, P. (1999). Src family kinases are required for integrin but not PDGFR signal transduction. EMBO J. *18*, 2459–2471.

Lee, H.S., Bellin, R.M., Walker, D.L., Patel, B., Powers, P., Liu, H., Garcia-Alvarez, B., de Pereda, J.M., Liddington, R.C., Volkmann, N., et al. (2004). Characterization of an actin-binding site within the talin FERM domain. J. Mol. Biol. *343*, 771–784.

Mayer, B.J., Hirai, H., and Sakai, R. (1995). Evidence that SH2 domains promote processive phosphorylation by protein-tyrosine kinases. Curr. Biol. *5*, 296–305.

Merkel, R., Nassoy, P., Leung, A., Ritchie, K., and Evans, E. (1999). Energy landscapes of receptor-ligand bonds explored with dynamic force spectroscopy. Nature *397*, 50–53.

Missbach, M., Jeschke, M., Feyen, J., Muller, K., Glatt, M., Green, J., and Susa, M. (1999). A novel inhibitor of the tyrosine kinase Src suppresses phosphorylation of its major cellular substrates and reduces bone resorption in vitro and in rodent models in vivo. Bone *24*, 437–449.

Miyake, I., Hakomori, Y., Misu, Y., Nakadate, H., Matsuura, N., Sakamoto, M., and Sakai, R. (2005). Domain-specific function of ShcC docking protein in neuroblastoma cells. Oncogene *24*, 3206–3215.

Nakamoto, T., Sakai, R., Honda, H., Ogawa, S., Ueno, H., Suzuki, T., Aizawa, S., Yazaki, Y., and Hirai, H. (1997). Requirements for localization of p130cas to focal adhesions. Mol. Cell. Biol. *17*, 3884–3897.

Oberhauser, A.F., Badilla-Fernandez, C., Carrion-Vazquez, M., and Fernandez, J.M. (2002). The mechanical hierarchies of fibronectin observed with single-molecule AFM. J. Mol. Biol. *319*, 433–447.

Okuda, M., Takahashi, M., Suero, J., Murry, C.E., Traub, O., Kawakatsu, H., and Berk, B.C. (1999). Shear stress stimulation of p130(cas) tyrosine phosphorylation requires calcium-dependent c-Src activation. J. Biol. Chem. *274*, 26803–26809.

Rief, M., Gautel, M., Oesterhelt, F., Fernandez, J.M., and Gaub, H.E. (1997). Reversible unfolding of individual titin immunoglobulin domains by AFM. Science *276*, 1109–1112.

Sakai, R., Iwamatsu, A., Hirano, N., Ogawa, S., Tanaka, T., Mano, H., Yazaki, Y., and Hirai, H. (1994). A novel signaling molecule, p130, forms stable complexes in vivo with v-Crk and v-Src in a tyrosine phosphorylation-dependent manner. EMBO J. *13*, 3748–3756.

Sakakibara, A., Ohba, Y., Kurokawa, K., Matsuda, M., and Hattori, S. (2002). Novel function of Chat in controlling cell adhesion via Cas-Crk-C3G-pathway-mediated Rap1 activation. J. Cell Sci. *115*, 4915–4924.

Sawada, Y., and Sheetz, M.P. (2002). Force transduction by Triton cytoskeletons. J. Cell Biol. *156*, 609–615.

Sawada, Y., Nakamura, K., Doi, K., Takeda, K., Tobiume, K., Saitoh, M., Morita, K., Komuro, I., De Vos, K., Sheetz, M., and Ichijo, H. (2001). Rap1 is involved in cell stretching modulation of p38 but not ERK or JNK MAP kinase. J. Cell Sci. *114*, 1221–1227.

Shin, N.Y., Dise, R.S., Schneider-Mergener, J., Ritchie, M.D., Kilkenny, D.M., and Hanks, S.K. (2004). Subsets of the major tyrosine phosphorylation sites in Crk-associated substrate (CAS) are sufficient to promote cell migration. J. Biol. Chem. *279*, 38331–38337.

Tamada, M., Sheetz, M.P., and Sawada, Y. (2004). Activation of a signaling cascade by cytoskeleton stretch. Dev. Cell *7*, 709–718.

Tang, D.D., and Tan, J. (2003). Role of Crk-associated substrate in the regulation of vascular smooth muscle contraction. Hypertension *42*, 858–863.

Thomas, S.M., and Brugge, J.S. (1997). Cellular functions regulated by Src family kinases. Annu. Rev. Cell Dev. Biol. *13*, 513–609.

Vogel, V., and Sheetz, M. (2006). Local force and geometry sensing regulate cell functions. Nat. Rev. Mol. Cell Biol. *7*, 265–275.

Wang, Y., Botvinick, E.L., Zhao, Y., Berns, M.W., Usami, S., Tsien, R.Y., and Chien, S. (2005). Visualizing the mechanical activation of Src. Nature *434*, 1040–1045.

Wisniewska, M., Bossenmaier, B., Georges, G., Hesse, F., Dangl, M., Kunkele, K.P., Ioannidis, I., Huber, R., and Engh, R.A. (2005). The 1.1 A resolution crystal structure of the p130cas SH3 domain and ramifications for ligand selectivity. J. Mol. Biol. *347*, 1005–1014.

Zhong, C., Chrzanowska-Wodnicka, M., Brown, J., Shaub, A., Belkin, A.M., and Burridge, K. (1998). Rho-mediated contractility exposes a cryptic site in fibronectin and induces fibronectin matrix assembly. J. Cell Biol. *141*, 539–551.

Vol 446|29 March 2007|doi:10.1038/nature05683

LETTERS

Dioxin receptor is a ligand-dependent E3 ubiquitin ligase

Fumiaki Ohtake[1,2], Atsushi Baba[2], Ichiro Takada[2], Maiko Okada[2], Kei Iwasaki[1], Hiromi Miki[2], Sayuri Takahashi[2,3], Alexander Kouzmenko[1,2], Keiko Nohara[4], Tomoki Chiba[5], Yoshiaki Fujii-Kuriyama[6,7] & Shigeaki Kato[1,2]

Fat-soluble ligands, including sex steroid hormones and environmental toxins, activate ligand-dependent DNA-sequence-specific transcriptional factors that transduce signals through target-gene-selective transcriptional regulation[1]. However, the mechanisms of cellular perception of fat-soluble ligand signals through other target-selective systems remain unclear. The ubiquitin–proteasome system regulates selective protein degradation, in which the E3 ubiquitin ligases determine target specificity[2–4]. Here we characterize a fat-soluble ligand-dependent ubiquitin ligase complex in human cell lines, in which dioxin receptor (AhR)[5–9] is integrated as a component of a novel cullin 4B ubiquitin ligase complex, $CUL4B^{AhR}$. Complex assembly and ubiquitin ligase activity of $CUL4B^{AhR}$ *in vitro* and *in vivo* are dependent on the AhR ligand. In the $CUL4B^{AhR}$ complex, ligand-activated AhR acts as a substrate-specific adaptor component that targets sex steroid receptors for degradation. Thus, our findings uncover a function for AhR as an atypical component of the ubiquitin ligase complex and demonstrate a non-genomic signalling pathway in which fat-soluble ligands regulate target-protein-selective degradation through a ubiquitin ligase complex.

The transcriptional regulatory system and the ubiquitin–proteasome system are two major target-selective systems that control intracellular protein levels. This target selectivity depends on the recognition of specific DNA elements by sequence-specific transcription factors[1] and the recognition of degradation substrates by E3 ubiquitin ligases[2–4]. These transcription factors and ligases serve primarily as specific adaptors that subsequently recruit transcriptional co-regulators and E2 ubiquitin-conjugating enzymes, respectively, to appropriate targets. The selective biological effects of fat-soluble ligands have been reported to be mediated by two classes of sequence-specific transcription factors, nuclear receptors[1] and arylhydrocarbon receptor (AhR) belonging to the basic helix–loop–helix (bHLH)/Per-Arnt-Sim (PAS) family[5–9].

AhR ligands modulate oestrogen and sex hormone, signalling both positively and negatively[8,10–13]. Functional impairments of male and female reproductive organs in AhR-deficient mice indicate the possible importance of AhR in sex hormone signalling[10,14]. Different AhR agonists[9], including 3-methylcholanthrene (3MC) and 2,3,7,8-tetrachlordibenzo-*p*-dioxin (TCDD), modulate oestrogen-dependent oestrogen receptor (ER)-α transactivation through the association of activated AhR/Arnt with ER-α[15]. Similarly, the transcriptional activity of nuclear androgen receptor (AR) was modulated by association with activated AhR (Supplementary Fig. S2a). However, ligand-bound AhR did not block oestrogen-induced co-activator recruitment on the oestrogen-responsive promoter (Supplementary Fig. S2b). This implies another mode of function for ligand-activated AhR beyond transcriptional regulation.

On activation of AhR by 3MC, we observed that protein levels of endogenous ER-α (in mammary tumour MCF-7 cells), ER-β (in ovarian tumour KGN cells) and AR (in prostate cancer LNCaP cells) were drastically decreased (Fig. 1a–c, and Supplementary Fig. 3a) without a change in messenger RNA levels (data not shown), irrespective of the presence of their cognate hormones. Other AhR agonists[9] (namely β-naphthoflavone (β-NF), environmental toxins such as TCDD and benzo[a]pyrene, and the endogenous metabolite indirubin) were similarly effective in protein degradation for ER-α (Fig. 1b) and ER-β/AR (data not shown), in agreement with a previous report on downregulated levels of uterine ER-α protein in rats treated with TCDD[16]. An AhR partial agonist/antagonist α-naphthoflavone (α-NF) was unable to accelerate the degradation of either AhR or ER-α (Fig. 1b, and Supplementary Fig. S3b).

AhR ligand-induced degradation (Fig. 1a–c) and functional repression (Supplementary Fig. S2c, d) of sex steroid receptors were abrogated in the presence of a proteasome inhibitor MG132. Consistently, poly-ubiquitination of ER-α was promoted by the activated AhR regardless of the presence of oestrogen (Fig. 1d, and Supplementary Fig. S3c). Pulse-chase kinetic analysis indicated that 3MC-induced degradation of ER-α was coupled to that of AhR[8,17,18] (Supplementary Fig. S3d). Moreover, the self-ubiquitination activity of the ligand-bound AhR immunocomplex was detected in an E1/E2-dependent manner (Supplementary Fig. S3e). Together with 3MC-dependent recognition of sex steroid receptors by AhR[8,12,13,15], these properties of AhR resemble those of classical adaptor components of the E3 ubiquitin ligase complexes, such as F-box proteins[3] or von Hippel–Lindau protein[19]. We therefore reasoned that activated AhR might act as an E3 ubiquitin ligase complex component.

To address this idea, AhR-containing complexes were purified from HeLa cells expressing Flag–AhR treated with 3MC or α-NF[15,20]. AhR formed large complexes in the presence of 3MC (Supplementary Fig. S4a–c). Further purification revealed five major 3MC-dependent complexes containing AhR (Fig. 1e). Complexes A and C contained well-known co-activators TRAP220/DRIP205/Med220 and p300 (ref. 1) (Supplementary Fig. S4d, e). Endogenous ER-α was detected in complexes B and C; however, ubiquitinated components were seen only in complex B (Fig. 1f, g).

Complex B was composed of the ubiquitin ligase core components cullin 4B (CUL4B)[3,21,22], damaged-DNA-binding protein 1 (DDB1)[23–27] and Rbx1 (Roc1)[3], together with subunits of the proteasomal 19S regulatory particle (19S RP), Arnt and transducin-β-like 3 (TBL3) (Fig. 1h). These components eluted with AhR in the presence of 3MC but not in the presence of α-NF (Fig. 1i, and Supplementary Fig. S4f). Neither CUL4A nor known substrate-specific adaptor components of CUL4A, such as DDB2, CSA and DET1[23,24], were present

[1]ERATO, Japan Science and Technology Agency, 4-1-8 Honcho, Kawaguchi, Saitama 332-0012, Japan. [2]Institute of Molecular and Cellular Biosciences, University of Tokyo, 1-1-1 Yayoi, Bunkyo-ku, Tokyo 113-0032, Japan. [3]Department of Urology, Faculty of Medicine, University of Tokyo, 7-3-1 Hongo, Bunkyo-ku, 113-8655, Japan. [4]National Institute for Environmental Studies, Tsukuba, Ibaraki 305-8506, Japan. [5]Graduate School of Life and Environmental Sciences, and [6]TARA Center, University of Tsukuba, 1-1-1 Tennodai Tsukuba, 305-8577, Japan. [7]SORST, Japan Science and Technology Agency, 4-1-8 Honcho, Kawaguchi, Saitama 332-0012, Japan.

in the AhR–CUL4B complex. As the cullin amino terminus binds adaptor components and the carboxy terminus interacts with an E2 enzyme-binding subunit Rbx1 (ref. 3), we performed tandem purification of the AhR–CUL4B complex with glutathione *S*-transferase (GST)-tagged CUL4B-N (N-terminal domain of CUL4B) and Flag–AhR. This led to the identification of a core complex consisting of five components: DDB1, AhR, Arnt, TBL3 and CUL4B (Fig. 1j). Together with Rbx1, this complex is denoted by $CUL4B^{AhR}$.

Immunoprecipitation of AhR together with endogenous CUL4B from MCF-7 and LNCaP cells was observed only in the presence of 3MC (Fig. 2a, b). Consistently, ligand-dependent co-localization of AhR with CUL4 was seen in MCF-7 cells (Fig. 2c). Whereas CUL4B seemed to act as a scaffold mediating DDB1–TBL3 and AhR–DDB1 interactions in $CUL4B^{AhR}$ (Fig. 2d, lane 4), ligand-activated AhR induced the assembly of complex components (Fig. 2d, lanes 1–3). DDB1 did not bridge CUL4B association with TBL3 or AhR, apparently because of the absence of the signature WDXR/DWD box[22,25–27] of either TBL3 or AhR, which is essential for DDB1 binding (Fig. 2d, lane 5, and Supplementary Fig. S5a). Consistently, specific and 3MC-dependent interaction of the conserved C-terminal acidic domain of AhR with the N-terminal region of CUL4B, but not with DDB1, was observed in a GST pulldown assay (Supplementary Figs S5b and S6). Because a constitutively active AhR mutant (AhRΔPASB)[9] interacted with CUL4B in the absence of ligand (Supplementary Fig. S5b), ligand-dependent structural alteration presumably induces AhR–CUL4B interaction. An AhR mutant lacking the CUL4B-binding

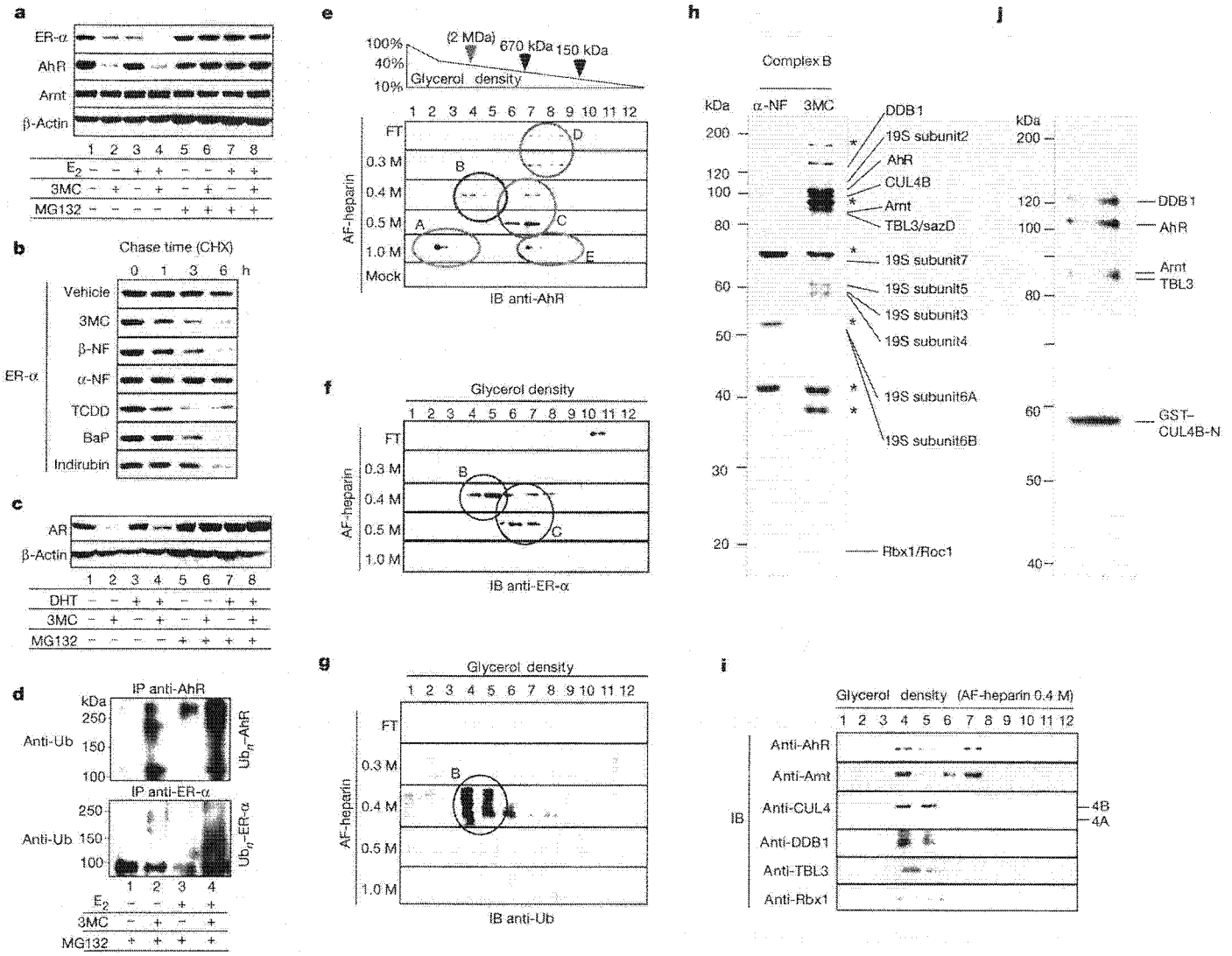

Figure 1 | Activated AhR acts as an E3 ubiquitin ligase. **a–c**, AhR-ligand-induced proteasomal degradation of ER-α (**a**, **b**) and AR (**c**). MCF-7 cells (**a**, **b**) and LNCaP cells (**c**) were incubated as indicated with E_2 (10 nM), DHT (10 nM) and/or 3MC (1 μM), β-NF (1 μM), benzo[a]pyrene (BaP; 100 nM), TCDD (10 nM), indirubin (10 nM) and α-NF (1 μM) in the presence or absence of MG132 (10 μM) and cycloheximide (CHX; 5 μM) for 3 h (**a**, **c**) or the indicated durations (**b**). Cell lysates were subjected to western blotting with specified antibodies. **d**, AhR-ligand-induced ubiquitination of ER-α. MCF-7 cells were incubated with the indicated ligands for 6 h. Western blots were subjected to dark exposure to detect poly-ubiquitinated forms of the receptors. IP, immunoprecipitation; Ub, ubiquitin. **e**, **f**, Biochemical separation and identification of AhR-associated complexes. Flag–AhR-associated proteins in the presence of 3MC or α-NF from HeLa cells stably expressing Flag–AhR were first fractionated by glycerol-density-gradient centrifugation (top, fractions 1–12), and then separated by Toyopearl AF-heparin column chromatography with the indicated KCl concentrations (FT, 1.0 M KCl). Samples from the 3MC-treated cells were resolved into five distinct complexes. IB, immunoblotting. **g**, Components of an AhR-associated complex are highly ubiquitinated. Western blots with anti-ubiquitin antibody. **h**, Identification of AhR-associated CUL4B ubiquitin ligase complex components. Components from complex B in **e** (fractions 4 and 5 from the glycerol-density-gradient centrifugation, eluted from an AF-heparin column at 0.4 M KCl) were resolved by SDS–PAGE, silver-stained and identified by matrix-assisted laser desorption ionization–time-of-flight MS analysis. **i**, Co-elution of the complex B components as a large complex. **j**, Association of activated AhR with the CUL4B complex. The $CUL4B^{AhR}$ complex from Flag–AhR-expressing HeLa cells treated with 3MC was affinity purified with GST-tagged N-terminal domain of CUL4B followed by anti-Flag antibody column fractionation.

acidic domain (AhRΔacid; Supplementary Fig. S6a) was indeed unable to promote ER-α ubiquitination *in vivo*, although the mutant retained 3MC-dependent transactivation function (Supplementary Fig. S5c). This indicates that the ubiquitin ligase function of AhR is independent of its transactivation function.

With two separately prepared components of recombinant AhR and CUL4B/DDB1/Rbx1 purified from *Spodoptera frugiperda* (Sf9) cells (Supplementary Fig. S7a), complex assembly *in vitro* was also dependent on 3MC (Fig. 2e). Furthermore, by *in vitro* ubiquitination assay (Supplementary Fig. S7b), the E3 ubiquitin ligase activity of $CUL4B^{AhR}$ for ER-α was dependent on 3MC but not on 17β-oestradiol (E_2) (Fig. 2f). These data indicate that both the complex assembly and the ubiquitin ligase activity of $CUL4B^{AhR}$ may be dependent on AhR agonists.

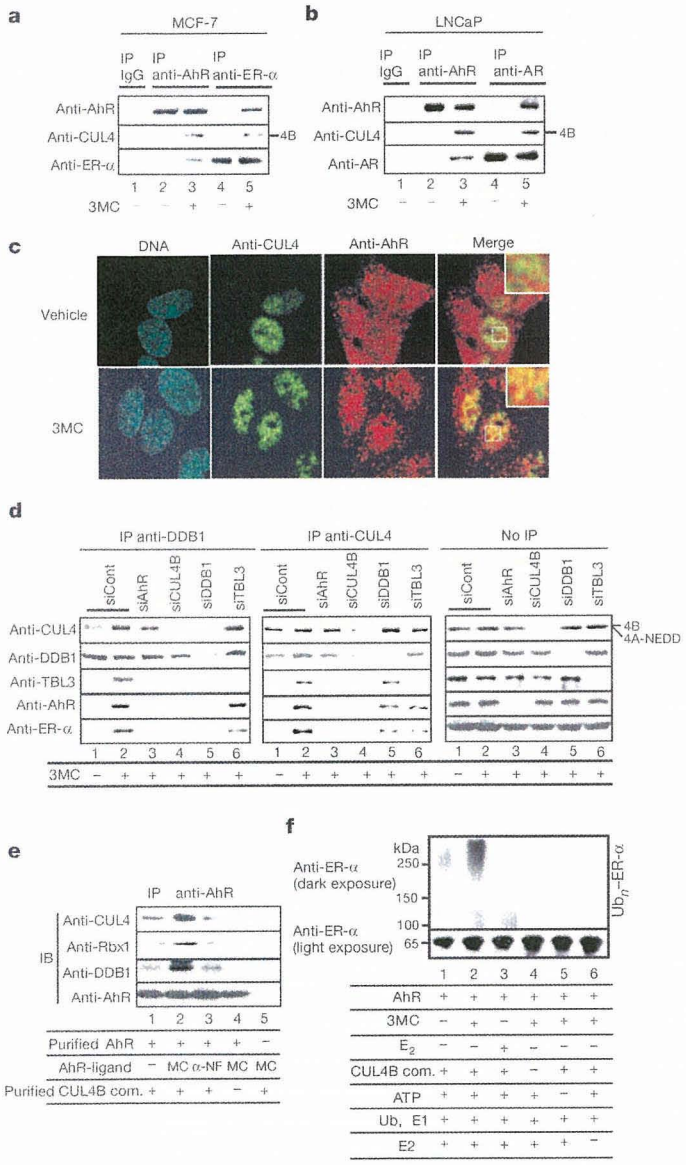

Figure 2 | AhR ligand-dependent assembly and ubiquitin ligase activity of $CUL4B^{AhR}$. **a**, **b**, 3MC-dependent association of endogenous CUL4B and AhR with ER-α and AR. Co-immunoprecipitation analyses from MCF-7 (**a**) and LNCaP (**b**) cells incubated with ligand and MG132 for 2 h. IP, immunoprecipitation. **c**, 3MC-dependent co-localization of AhR with CUL4. MCF-7 cells incubated with 3MC and MG132 for 2 h were immunostained with the indicated antibodies. **d**, Formation of the $CUL4B^{AhR}$ complex. MCF-7 cells were transfected with specified short interfering RNAs (siRNAs) for 48 h, treated with 3MC and MG132 for 2 h, and immunoprecipitated with the indicated antibodies. **e**, Assembly of the CUL4B complex components with AhR is dependent on 3MC *in vitro*. Immunoprecipitation with anti-AhR antibodies of the indicated recombinant CUL4B complex components (CUL4B com.) was observed only in the presence of 3MC. IB, immunoblotting. **f**, $CUL4B^{AhR}$ ubiquitinates ER-α *in vitro*. ER-α protein was incubated with and without recombinant $CUL4B^{AhR}$ E3 complex components, ubiquitin (Ub), ATP, E1 and E2 enzymes as indicated, then subjected to western blotting.

We then examined whether the recognition of sex steroid receptors for 3MC-dependent ubiquitination is indeed mediated by AhR. Co-immunoprecipitation analyses indicated that ligand-activated AhR was required for the recruitment of ER-α (Fig. 2a, d) or AR (Fig. 2b, and data not shown) to $CUL4B^{AhR}$. TBL3 and DDB1 did not seem essential for ER-α recruitment but stabilized the association of ER-α with $CUL4B^{AhR}$ (Fig. 2d). Moreover, knockdown of $CUL4B^{AhR}$ components (Supplementary Fig. S8) impaired the 3MC-induced ubiquitination and degradation of ER-α (Fig. 3a–d, and Supplementary Fig. S9a, b) and AR (Fig. 3e, Supplementary Fig. S9c and data not shown), and abolished the AhR-ligand-induced repression of ER-α transactivation (Supplementary Fig. S10a). Recognition of ER-α by activated AhR was retained, but ubiquitination of AhR-bound ER-α was abrogated, by knockdown of the other $CUL4B^{AhR}$ components (Fig. 3d). An ER-α ΔA/B mutant[15] that lacks interaction with AhR, and an ER-α K7R mutant in which seven lysine residues had been replaced with arginine (Supplementary Fig. S6b), were resistant to AhR-dependent ubiquitination and transrepression (Fig. 3f, and Supplementary Fig. S10b). Taken together, these data suggest that ligand-activated AhR functions as a substrate-specific adaptor component of $CUL4B^{AhR}$. AhR is therefore a unique and atypical substrate-specific component of a cullin-based E3 complex, because AhR bears no known interaction motif with cullin complexes yet associates directly with CUL4B. Ubiquitination of ER-α-associated AhR was similarly abolished by the knockdown, and the overall ubiquitination and degradation of AhR[8,17,18] were partly affected (Supplementary Fig. S11a, b). This implies the existence of $CUL4B^{AhR}$-dependent (self-ubiquitination[3]) and $CUL4B^{AhR}$-independent pathways for AhR degradation.

Human ER-α (hER-α) degradation is reportedly accelerated by the binding of E_2 (ref. 1) or the phosphorylation of Ser 118 (ref. 28), whereas a partial antagonist, tamoxifen, has been shown to stabilize ER-α[1]. Nevertheless, 3MC-activated AhR efficiently induced the ubiquitination and subsequent degradation of tamoxifen-bound ER-α and ER-α-S118A mutant (Fig. 3f). Reciprocally, AhR was dispensable for E_2-dependent ER-α degradation (Supplementary Fig. S11c). These results indicate that the $CUL4B^{AhR}$ system may act independently of innate protein degradation system(s) for ER-α. XAP2/ARA9/AIP[7,8,17], a chaperone that modulates the stability of unliganded AhR, seemed unlikely to mediate the accelerated degradation of ER-α by activated AhR (Supplementary Fig. S11d).

Last, we addressed the physiological significance of $CUL4B^{AhR}$ for sex hormone signalling in intact animals. Injection with either 3MC (Fig. 4a) or β-NF (Fig. 4c) did not affect the expression of ER-α or AR mRNA (data not shown) but caused a decrease in protein levels of uterine ER-α in ovariectomized female wild-type mice and of prostate AR in castrated male wild-type mice (Fig. 4b) regardless of their treatment with cognate sex hormones. However, AhR deficiency ($AhR^{-/-}$ mice)[9,14] abolished such effects of AhR ligands but did not affect the modulation of stability of sex steroid receptors by their respective hormones (Fig. 4a, b). As a result of reduced sex steroid receptor levels after pretreatment with 3MC, E_2-dependent induction of c-*fos* in the uterus[15] and dihydrotestosterone (DHT)-dependent induction of *Probasin* in the prostate[10] were severely impaired (Fig. 4a, b). Cellular proliferation and gene induction in response to sex hormones in primary cultured epithelial cells from normal mouse uterus and prostate were consistently suppressed by 3MC (Supplementary Fig. S12a, b) and β-NF (Supplementary Fig. S12c), but no effect was detected in $AhR^{-/-}$ cells (Supplementary Fig. S12a, b). The significance of $CUL4B^{AhR}$ complex components in the AhR-mediated suppression of sex hormone effects

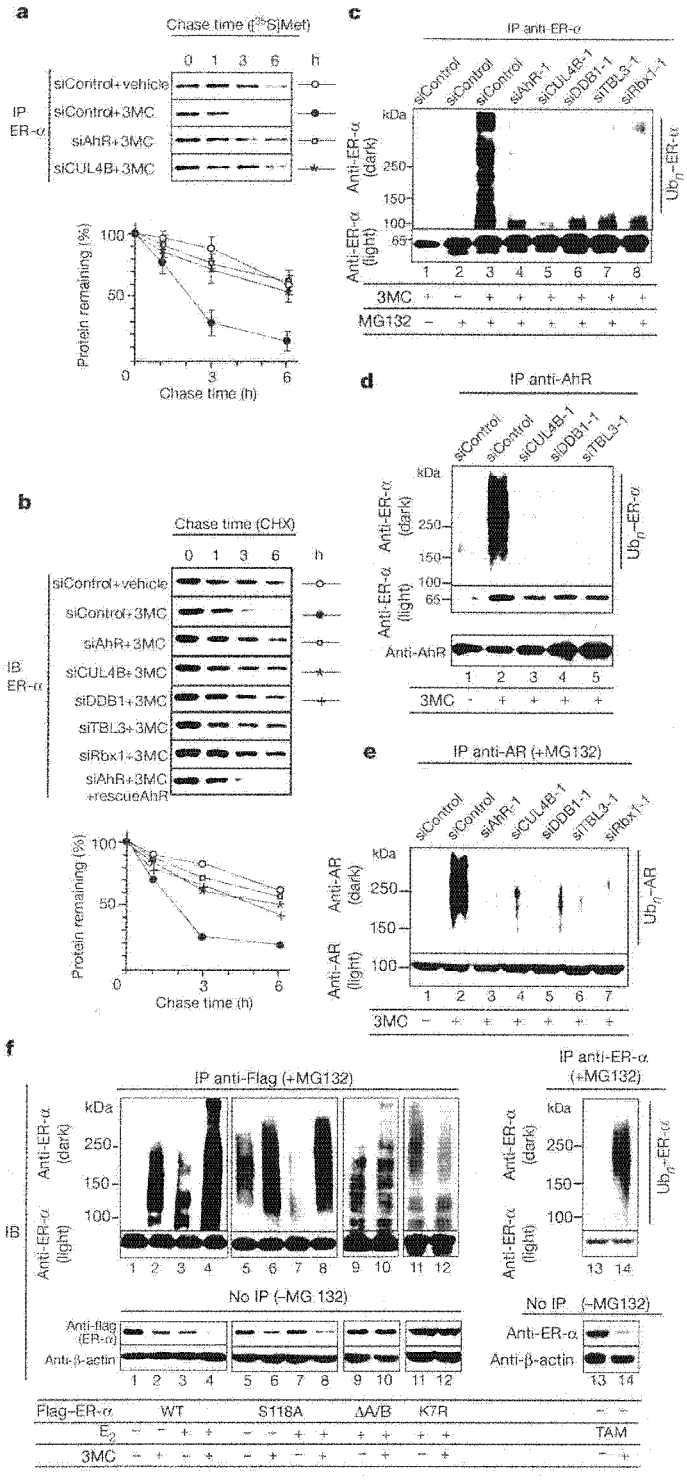

Figure 3 | Activated AhR is a substrate-specific adaptor component of the CUL4B^{AhR} complex. **a**–**c**, Components of CUL4B^{AhR} are required for 3MC-dependent ubiquitination and degradation of ER-α. MCF-7 cells were transfected with indicated siRNAs for 48 h, then used in pulse-chase analysis as in Supplementary Fig. S3d (**a**), in cycloheximide (CHX) chasing (**b**) and in the *in vivo* ubiquitination assay with ligand incubation for 6 h (**c**). All values are shown as means ± s.d. ($n = 3$) (**a**) or as means ($n = 3$) (**b**). The knockdown efficiency in the same lysates was confirmed in Supplementary Fig. S9a. IB, immunoblotting; IP, immunoprecipitation. **d**, AhR is the substrate-specific adaptor in the targeting of ER-α by CUL4B^{AhR}. MCF-7 cells transfected with the indicated siRNAs were lysed in TNE buffer and immunoprecipitated with anti-AhR antibody in the presence of MG132. Ubiquitination of the ER-α co-immunoprecipitated with AhR was detected by western blotting. **e**, LNCaP cells were subjected to the same analysis as in **a**–**c**. **f**, AhR-ligand-induced ER-α ubiquitination requires intact lysine residues and is independent of oestrogen binding or S118 phosphorylation of hER-α. Intact MCF-7 cells (right) or cells transfected with Flag–hER-α, AhR and their derivatives (left) were treated with the indicated ligands in the presence (top) or absence (bottom) of MG132 for 6 h, then subjected to western blotting. TAM, tamoxifen; WT, wild type.

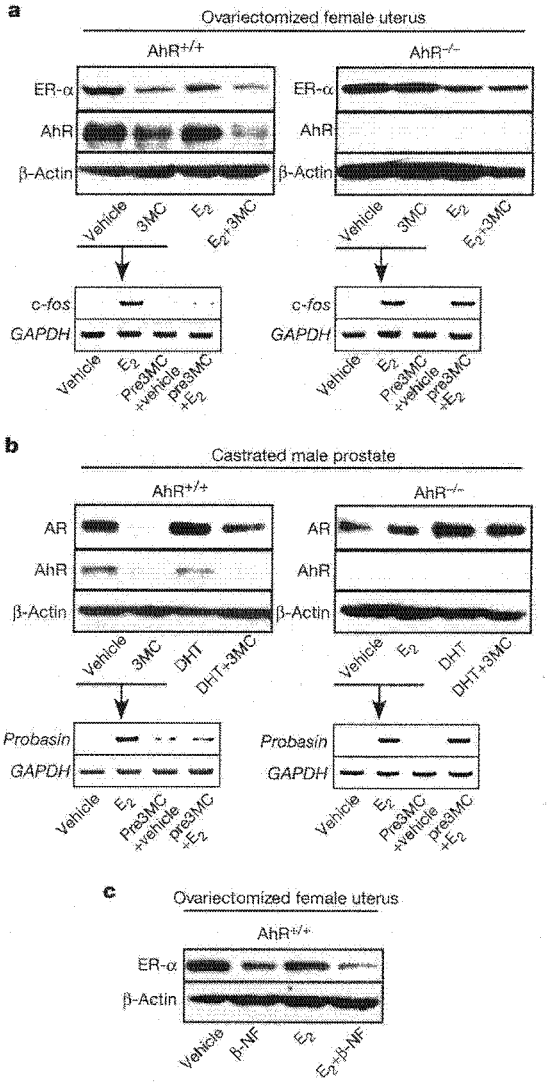

Figure 4 | Ligand-dependent ubiquitin ligase function of AhR *in vivo*. **a**, **b**, AhR activation enhances the degradation of ER-α and AR *in vivo*. Top: nine-week-old ovariectomized female mice (**a**) or castrated male mice (**b**) of the indicated genotypes were injected with vehicle or indicated ligands. After 4 h, uterus (**a**) or ventral prostate (**b**) was isolated and subjected to western blotting. Bottom: mice pretreated with vehicle or 3MC for 8 h were injected with either vehicle or E_2 (**a**), or DHT (**b**). After 4 h, the uterus or prostate was isolated for reverse transcriptase PCR. GAPDH, glyceraldehyde-3-phosphate dehydrogenase. **c**, Other AhR agonists produce a similar effect on oestrogen signalling to that of 3MC.

(Supplementary Fig. S12a, b) and the promotion of ER-α degradation in uterine cells (Supplementary Fig. S12d) was verified by knockdown of the components.

Here we have shown that a known sequence-specific transcription factor AhR acts as a ligand-dependent CUL4B-based E3 ubiquitin ligase for selectively targeting sex steroid receptors to bring about accelerated protein degradation. The transcription and ubiquitination functions of AhR seem to be responsible for a distinct set of biological events caused by endogenous and exogenous AhR ligands. In ubiquitin ligase complexes, substrate recognition by known

substrate-specific components is generally evoked by substrate modifications[2–4]. However, the recognition and subsequent ubiquitination of sex steroid receptors by AhR requires dioxin-type compounds as ligands but does not require the phosphorylation or ligand binding of sex steroid receptors. We have therefore shown that fat-soluble ligands directly control the function of a ubiquitin ligase complex for targeted protein destruction in animals (see Supplementary Fig. S1). In plants, auxin was recently found to control protein destruction through the auxin receptor SCF^{TIR1} (refs 29, 30). However, whereas SCF^{TIR1} is regulated by ligand-dependent substrate recognition by TIR1, $CUL4B^{AhR}$ is primarily regulated by the assembly of a ligand-dependent complex as well as substrate recognition. Considered together, ubiquitin-ligase-based perception mechanisms of fat-soluble ligands may be diverse in different species. It is possible that other nuclear receptors and binding proteins for fat-soluble ligands also serve as key components of ubiquitin ligases to mediate a non-genomic pathway of fat-soluble ligands to regulate target-protein-selective destruction.

METHODS

More detailed descriptions of all materials and methods are supplied in the Supplementary Information.

Biochemical purification and separation of AhR-associated complexes. The nuclear extracts preparation, anti-Flag affinity purification and mass spectrometry were performed as described previously[15,20]. For purification of the core $CUL4B^{AhR}$ complex, the nuclear extracts were first bound to the GST–CUL4B-N (amino acid residues 1–318) columns before being loaded on anti-Flag columns[20].

***In vitro* ubiquitination assay.** The *in vitro* ubiquitination assay was performed as described previously[15]. Purified Flag–AhR (0.2 μg) was incubated either with 3MC (10 μM) or vehicle (dimethylsulphoxide) for 30 min at 25 °C, then mixed with Flag–CUL4B/DDB1/Rbx1 complex (0.2 μg), and after further incubation for 30 min at 25 °C the substrate, ER-α (Calbiochem), was added.

Plasmids, antibodies, immunoprecipitation, *in vivo* ubiquitination, pulse-chasing, ligand responses in mice, and RNA-mediated interference experiments. Detailed methods used in this study can be found in the Supplementary Information.

Received 13 December 2006; accepted 16 February 2007.

1. McKenna, N. J. & O'Malley, B. W. Combinatorial control of gene expression by nuclear receptors and coregulators. *Cell* 108, 465–474 (2002).
2. Hershko, A. & Ciechanover, A. The ubiquitin system. *Annu. Rev. Biochem.* 67, 425–479 (1998).
3. Deshaies, R. J. SCF and Cullin/Ring H2-based ubiquitin ligases. *Annu. Rev. Cell Dev. Biol.* 15, 435–467 (1999).
4. Harper, J. W. A phosphorylation-driven ubiquitination switch for cell-cycle control. *Trends Cell Biol.* 12, 104–107 (2002).
5. Poellinger, L. Mechanistic aspects—the dioxin (aryl hydrocarbon) receptor. *Food Addit. Contam.* 17, 261–266 (2000).
6. Hankinson, O. The aryl hydrocarbon receptor complex. *Annu. Rev. Pharmacol. Toxicol.* 35, 307–340 (1995).
7. Swanson, H. I. & Bradfield, C. A. The AH-receptor: genetics, structure and function. *Pharmacogenetics* 3, 213–230 (1993).
8. Carlson, D. B. & Perdew, G. H. A dynamic role for the Ah receptor in cell signaling? Insights from a diverse group of Ah receptor interacting proteins. *J. Biochem. Mol. Toxicol.* 16, 317–325 (2002).
9. Mimura, J. & Fujii-Kuriyama, Y. Functional role of AhR in the expression of toxic effects by TCDD. *Biochim. Biophys. Acta* 1619, 263–268 (2003).
10. Lin, T. M. *et al.* Effects of aryl hydrocarbon receptor null mutation and in utero and lactational 2,3,7,8-tetrachlorodibenzo-*p*-dioxin exposure on prostate and seminal vesicle development in C57BL/6 mice. *Toxicol. Sci.* 68, 479–487 (2002).
11. Brunnberg, S. *et al.* The basic helix-loop-helix-PAS protein ARNT functions as a potent coactivator of estrogen receptor-dependent transcription. *Proc. Natl Acad. Sci. USA* 100, 6517–6522 (2003).
12. Matthews, J., Wihlen, B., Thomsen, J. & Gustafsson, J. A. Aryl hydrocarbon receptor-mediated transcription: ligand-dependent recruitment of estrogen receptor α to 2,3,7,8-tetrachlorodibenzo-*p*-dioxin-responsive promoters. *Mol. Cell. Biol.* 25, 5317–5328 (2005).
13. Beischlag, T. V. & Perdew, G. H. ER α–AHR–ARNT protein–protein interactions mediate estradiol-dependent transrepression of dioxin-inducible gene transcription. *J. Biol. Chem.* 280, 21607–21611 (2005).
14. Baba, T. *et al.* Intrinsic function of the aryl hydrocarbon (dioxin) receptor as a key factor in female reproduction. *Mol. Cell. Biol.* 25, 10040–10051 (2005).
15. Ohtake, F. *et al.* Modulation of oestrogen receptor signalling by association with the activated dioxin receptor. *Nature* 423, 545–550 (2003).
16. Romkes, M., Piskorska-Pliszczynska, J. & Safe, S. Effects of 2,3,7,8-tetrachlorodibenzo-*p*-dioxin on hepatic and uterine estrogen receptor levels in rats. *Toxicol. Appl. Pharmacol.* 87, 306–314 (1987).
17. Davarinos, N. A. & Pollenz, R. S. Aryl hydrocarbon receptor imported into the nucleus following ligand binding is rapidly degraded via the cytosplasmic proteasome following nuclear export. *J. Biol. Chem.* 274, 28708–28715 (1999).
18. Roberts, B. J. & Whitelaw, M. L. Degradation of the basic helix–loop–helix/Per-ARNT-Sim homology domain dioxin receptor via the ubiquitin/proteasome pathway. *J. Biol. Chem.* 274, 36351–36356 (1999).
19. Maxwell, P. H. *et al.* The tumour suppressor protein VHL targets hypoxia-inducible factors for oxygen-dependent proteolysis. *Nature* 399, 271–275 (1999).
20. Kitagawa, H. *et al.* The chromatin-remodeling complex WINAC targets a nuclear receptor to promoters and is impaired in Williams syndrome. *Cell* 113, 905–917 (2003).
21. Zhong, W., Feng, H., Santiago, F. E. & Kipreos, E. T. CUL-4 ubiquitin ligase maintains genome stability by restraining DNA-replication licensing. *Nature* 423, 885–889 (2003).
22. Higa, L. A. *et al.* CUL4–DDB1 ubiquitin ligase interacts with multiple WD40-repeat proteins and regulates histone methylation. *Nature Cell Biol.* 8, 1277–1283 (2006).
23. Groisman, R. *et al.* The ubiquitin ligase activity in the DDB2 and CSA complexes is differentially regulated by the COP9 signalosome in response to DNA damage. *Cell* 113, 357–367 (2003).
24. Wertz, I. E. *et al.* Human De-etiolated-1 regulates c-Jun by assembling a CUL4A ubiquitin ligase. *Science* 303, 1371–1374 (2004).
25. Jin, J., Arias, E. E., Chen, J., Harper, J. W. & Walter, J. C. A family of diverse Cul4-Ddb1-interacting proteins includes Cdt2, which is required for S phase destruction of the replication factor Cdt1. *Mol. Cell* 23, 709–721 (2006).
26. Angers, S. *et al.* Molecular architecture and assembly of the DDB1–CUL4A ubiquitin ligase machinery. *Nature* 443, 590–593 (2006).
27. He, Y. J., McCall, C. M., Hu, J., Zeng, Y. & Xiong, Y. DDB1 functions as a linker to recruit receptor WD40 proteins to CUL4–ROC1 ubiquitin ligases. *Genes Dev.* 20, 2949–2954 (2006).
28. Valley, C. C. *et al.* Differential regulation of estrogen-inducible proteolysis and transcription by the estrogen receptor alpha N terminus. *Mol. Cell. Biol.* 25, 5417–5428 (2005).
29. Dharmasiri, N., Dharmasiri, S. & Estelle, M. The F-box protein TIR1 is an auxin receptor. *Nature* 435, 441–445 (2005).
30. Kepinski, S. & Leyser, O. The *Arabidopsis* F-box protein TIR1 is an auxin receptor. *Nature* 435, 446–451 (2005).

Supplementary Information is linked to the online version of the paper at www.nature.com/nature.

Acknowledgements We thank K. Tanaka, C. K. Glass, J. Yanagisawa, Y. Gotoh and J. Mimura for comments; S. Murata, T. Matsuda, T. Suzuki and Y. Tateishi for providing materials; T. Matsumoto, M. Igarashi and S. Fujiyama for technical assistance; and H. Higuchi for manuscript preparation. This work was supported in part by the Program for Promotion of Basic Research Activities for Innovative Biosciences (PROBRAIN) and priority areas from the Ministry of Education, Culture, Sports, Science and Technology (to Y.F.-K. and S.K.).

Author Contributions F.O., T.C., Y.F.-K. and S.K. designed the experiments. F.O., A B., M.O., K I., H.M., S.T. and I. T. performed the experiments. F.O., A.K. and S.K. wrote the paper.

Author Information Reprints and permissions information is available at www.nature.com/reprints. The authors declare no competing financial interests. Correspondence and requests for materials should be addressed to S.K. (uskato@mail.ecc.u-tokyo.ac.jp).

doi:10.1038/nature05732

TRIM25 RING-finger E3 ubiquitin ligase is essential for RIG-I-mediated antiviral activity

Michaela U. Gack[1,2], Young C. Shin[1], Chul-Hyun Joo[1,3], Tomohiko Urano[4,5], Chengyu Liang[1], Lijun Sun[6], Takeuchi Osamu[7], Shizuo Akira[7], Zhijian Chen[6], Satoshi Inoue[4,5] & Jae U. Jung[1]

Retinoic-acid-inducible gene-I (RIG-I; also called DDX58) is a cytosolic viral RNA receptor that interacts with MAVS (also called VISA, IPS-1 or Cardif) to induce type I interferon-mediated host protective innate immunity against viral infection[1–6]. Furthermore, members of the tripartite motif (TRIM) protein family, which contain a cluster of a RING-finger domain, a B box/coiled-coil domain and a SPRY domain, are involved in various cellular processes, including cell proliferation and antiviral activity[7]. Here we report that the amino-terminal caspase recruitment domains (CARDs) of RIG-I undergo robust ubiquitination induced by TRIM25 in mammalian cells. The carboxy-terminal SPRY domain of TRIM25 interacts with the N-terminal CARDs of RIG-I; this interaction effectively delivers the Lys 63-linked ubiquitin moiety to the N-terminal CARDs of RIG-I, resulting in a marked increase in RIG-I downstream signalling activity. The Lys 172 residue of RIG-I is critical for efficient TRIM25-mediated ubiquitination and for MAVS binding, as well as the ability of RIG-I to induce antiviral signal transduction. Furthermore, gene targeting demonstrates that TRIM25 is essential not only for RIG-I ubiquitination but also for RIG-I-mediated interferon-β production and antiviral activity in response to RNA virus infection. Thus, we demonstrate that TRIM25 E3 ubiquitin ligase induces the Lys 63-linked ubiquitination of RIG-I, which is crucial for the cytosolic RIG-I signalling pathway to elicit host antiviral innate immunity.

A recent series of studies has identified RIG-I and melanoma differentiation-associated gene 5 (MDA5; also called IFIH1) as cytosolic receptors for viral double-stranded RNA and 5′ triphosphate RNA[2,4,6]. RIG-I and MDA5 belong to the DExD/H box RNA helicase family, the members of which contain two caspase recruitment domains (2CARD) in the N-terminal region and a potential ATP-dependent RNA helicase activity in the C-terminal region[8,9]. To decipher the cytosolic RIG-I-mediated antiviral signalling pathway, we attempted to identify cellular proteins associated with the N-terminal 2CARD of RIG-I and MDA5 using mammalian glutathione *S*-transferase (GST) fusion constructs. Polypeptides with apparent molecular masses of 52, 60 and 68 kDa were present specifically in the GST–RIG-I(2CARD) complex but not in the GST–MDA5(2CARD) complex or with GST alone (Fig. 1a). Notably, mass spectrometry and immunoblotting showed that these polypeptides were exclusively identified as ubiquitinated forms of GST–RIG-I(2CARD) (Supplementary Fig. 1a). To confirm RIG-I ubiquitination, HEK293T cells were co-transfected with Flag-tagged full-length RIG-I or a RIG-I mutant in which the 2CARD had been deleted (RIG-I(Δ2CARD)) together with haemagglutinin (HA)-tagged ubiquitin. RIG-I, but not RIG-I(Δ2CARD), was extensively ubiquitinated (Fig. 1b and Supplementary Fig. 1b). In addition, anti-HA immunoblotting detected ubiquitinated Flag-tagged RIG-I as multiple species with apparent molecular masses of 120–150 kDa, significantly larger than unmodified Flag–RIG-I (Fig. 1c, top left panel). Furthermore, Sendai virus infection and/or interferon (IFN)-β treatment resulted in the markedly increased ubiquitination of endogenously or exogenously expressed RIG-I (Fig. 1c and Supplementary Fig. 1c). These results indicate that RIG-I undergoes robust ubiquitination at its N-terminal 2CARD and that this ubiquitination apparently increases on viral infection.

To dissect further the ubiquitination of the 2CARD of RIG-I, which contains 18 lysine residues, the *in vivo* ubiquitinated forms of N-terminal GST-fused and C-terminal Flag-tagged RIG-I(2CARD) were purified and analysed by multi-dimensional liquid chromatography coupled with tandem mass spectrometry (LC/LC-MS/MS; Fig. 1a, d, bands 1–3). Both GST–RIG-I(2CARD) and Flag–RIG-I(2CARD) carried the ubiquitin peptides at Lys 99, 169, 172, 181, 190 or 193 (Fig. 1d). Additional mass spectrometry analysis showed that band 2 and 3 fragments carried the unique, branched Gly-Gly signature peptides primarily with the ubiquitin Lys 63 linkage (Fig. 1d). Furthermore, GST–RIG-I(2CARD) and full-length RIG-I were strongly ubiquitinated when HA-tagged wild-type ubiquitin or a K48R ubiquitin mutant was expressed, whereas their ubiquitination was significantly reduced upon expression of a K63R ubiquitin mutant protein (Supplementary Fig. 2). These results indicate that the second CARD of RIG-I is the primary site for Lys 63-linked ubiquitination.

To corroborate the ubiquitination of the 2CARD of RIG-I, six lysine residues were replaced with arginine (K→R) individually and in various combinations; these mutants were then tested for their ubiquitination level. The K172R mutation (alone or together with other mutations) caused near-complete loss of ubiquitination of the 2CARD of RIG-I (Fig. 1e and Supplementary Fig. 3a). In contrast, other K→R mutations had little or no effect on ubiquitination of the RIG-I 2CARD (Fig. 1e). As previously shown[10], wild-type GST–RIG-I(2CARD) potently induced IFN-β and NF-κB promoter activity (Fig. 1f and Supplementary Fig. 3b). GST–RIG-I(2CARD) mutants containing the K172R mutation alone or together with other mutations showed markedly reduced IFN-β and NF-κB promoter activation, consistent with their lack of ubiquitination; in contrast, other GST–RIG-I(2CARD) mutants induced IFN-β and NF-κB promoter activity as strongly as wild-type GST–RIG-I(2CARD) (Fig. 1f and Supplementary Fig. 3b). These results suggest that Lys 172 is the essential site for RIG-I 2CARD ubiquitination and signalling activity

[1]Department of Microbiology and Molecular Genetics and Tumor Virology Division, New England Primate Research Center, Harvard Medical School, 1 Pine Hill Drive, Southborough, Massachusetts 01772, USA. [2]Institute for Clinical and Molecular Virology, Friedrich-Alexander University Erlangen-Nuremberg, 91054 Erlangen, Germany. [3]Department of Microbiology, University of Ulsan College of Medicine, Seoul 138-736, South Korea. [4]Department of Geriatric Medicine, Graduate School of Medicine, The University of Tokyo, 7-3-1 Hongo, Bunkyo, Tokyo 113-8655, Japan. [5]Research Center for Genomic Medicine, Saitama Medical School, Saitama 350-124-2, Japan. [6]Department of Molecular Biology, University of Texas Southwestern Medical Center, Dallas, Texas 75390-9148, USA. [7]Department of Host Defense, Japan Science and Technology Agency, Osaka 565-0871, Japan.

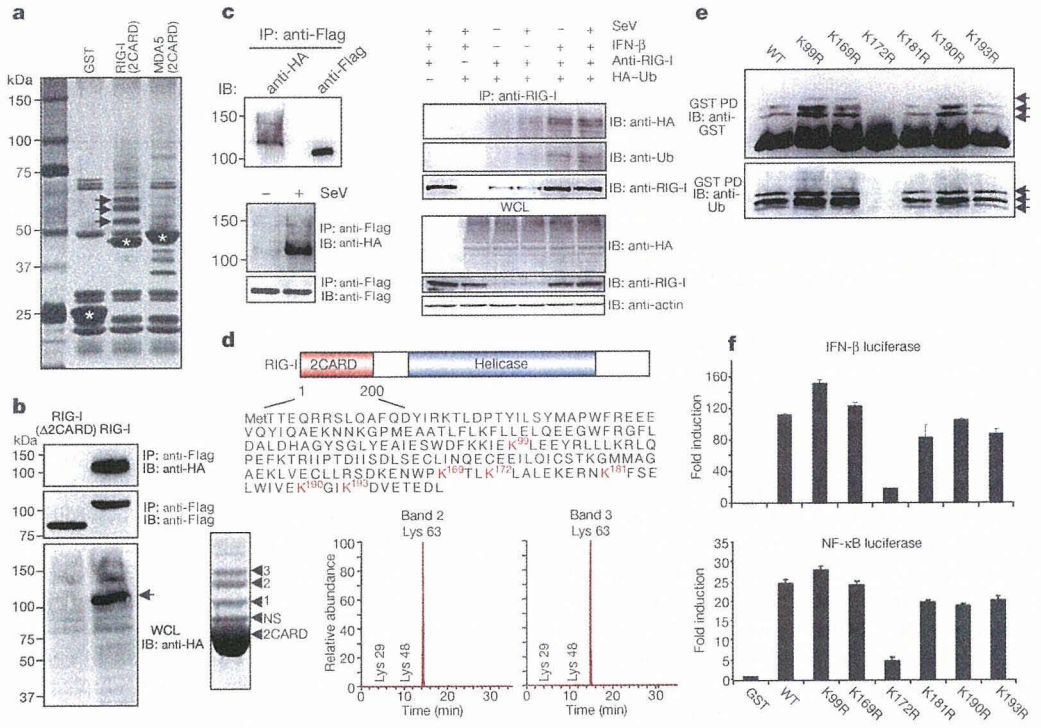

Figure 1 | The 2CARD of RIG-I undergoes robust ubiquitination. a, Silver-stained purified GST fusion complexes. Arrows, unique bands; asterisks, GST fusions. **b**, **c**, HEK293T cells transfected with Flag–RIG-I (**b**, and **c**, top-left) or Flag–RIG-I(Δ2CARD) (**b**) together with HA–ubiquitin were used for immunoprecipitation (IP) and immunoblotting (IB). WCL, whole cell lysate. **c**, Bottom-left panel: HEK293T cells transfected with Flag–RIG-I and HA–ubiquitin were mock-infected or infected with Sendai virus (SeV). Right: HEK293T cells transfected with HA–ubiquitin were treated (or not) with IFN-β and/or infected, as indicated, with Sendai virus before immunoprecipitation with anti-RIG-I antibody. **d**, The red lysine residues indicate the sites of ubiquitination. Bottom-left panel: Coomassie-blue-stained Flag–RIG-I(2CARD) complex. NS, nonspecific protein. Bottom-right panel: Lys 29/48/63-linked ubiquitination of RIG-I(2CARD)[21]. **e**, GST pull down (PD) of HEK293T cells transfected with GST–RIG-I(2CARD) or K→R mutants. Arrows indicate the ubiquitinated bands. WT, wild type. **f**, IFN-β and NF-κB promoter activity in GST–RIG-I(2CARD) or K→R mutant transfected cells. The results are expressed as means ± s.d. ($n = 3$).

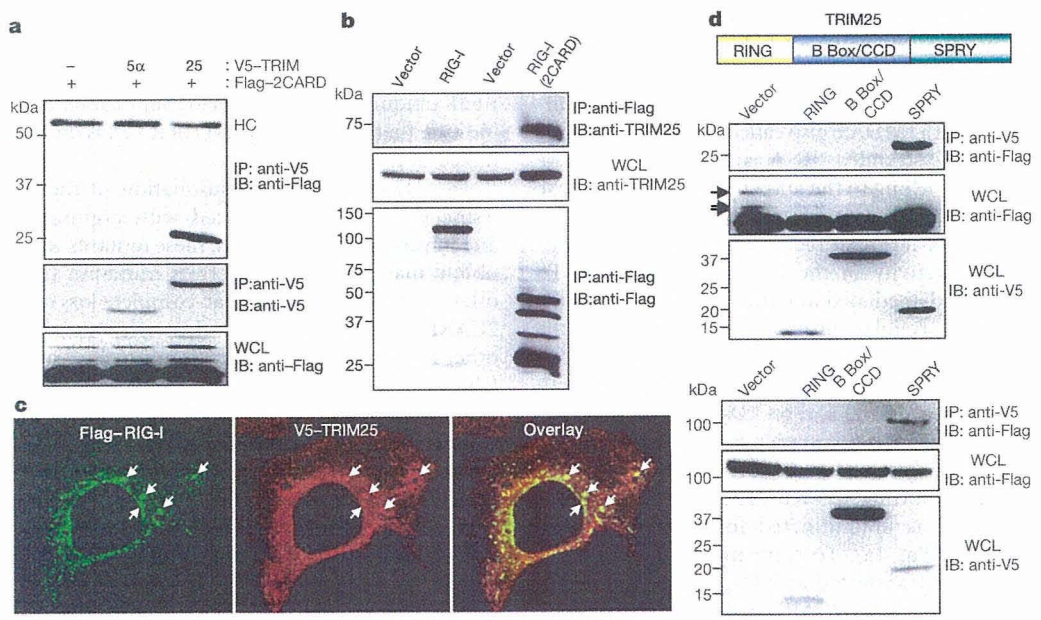

Figure 2 | Interaction between RIG-I and TRIM25. a, **b**, WCLs of HEK293T cells transfected with Flag–RIG-I(2CARD) and V5–TRIM25 or V5–TRIM5-α (**a**), or with Flag-RIG-I or Flag-RIG-I(2CARD) (**b**) were used for immunoprecipitation and immunoblotting, as indicated. **c**, Confocal images of Hela cells transiently transfected with Flag–RIG-I (green) and V5–TRIM25 (red). Arrows indicate representative co-localization between Flag–RIG-I and V5–TRIM25. Original magnification, ×100. **d**, WCLs of HEK293T cells transfected with Flag-tagged RIG-I(2CARD) (top) or full-length Flag–RIG-I (bottom) together with V5-tagged domains of TRIM25 were used for immunoprecipitation with V5 antibody, followed by immunoblotting with anti-Flag. WCLs were used for immunoblotting with anti-Flag and anti-V5 antibodies.

and that the extent of RIG-I 2CARD ubiquitination correlates strongly with its signal transduction activity.

Protein purification and mass spectrometry demonstrated that TRIM25 (also called oestrogen-responsive finger protein (EFP)[11]) is one of the proteins that associates with Flag–RIG-I(2CARD). TRIM25 has ubiquitin and ISG15 E3 ligase activity and downregulates 14-3-3σ through proteolysis for cell cycle regulation[12,13]. Co-immunoprecipitation revealed that RIG-I(2CARD) interacts with TRIM25 but not TRIM5-α, which has a similar structure to TRIM25 and functions as an intracellular inhibitor of retroviral replication[7] (Fig. 2a). Furthermore, interaction between Flag-tagged RIG-I or RIG-I(2CARD) and endogenous TRIM25 was readily detected in HEK293T cells (Fig. 2b). Confocal microscopy revealed that both RIG-I and TRIM25 exhibited punctate staining throughout the cytoplasm and that they co-localized extensively at cytoplasmic perinuclear bodies (Fig. 2c). As with other TRIM family members[7], TRIM25 contains a cluster of a RING-finger domain, a B box/coiled-coil domain (B Box/CCD) and a SPRY domain (Fig. 2d). Binding analysis revealed that the C-terminal SPRY domain of TRIM25 bound to both RIG-I and RIG-I(2CARD) as effectively as full-length TRIM25, whereas the RING-finger domain and B Box/CCD did not (Fig. 2d).

To test the role of TRIM25 in RIG-I ubiquitination, RIG-I or GST–RIG-I(2CARD) was co-expressed with wild-type TRIM25, E3 ligase-defective TRIM25(ΔRING) or TRIM5-α. TRIM25 expression markedly increased the ubiquitination levels of exogenous RIG-I and GST–RIG-I(2CARD), as well as endogenous RIG-I, but neither TRIM25(ΔRING) nor TRIM5-α had any effect (Fig. 3a, b; see also Supplementary Fig. 4a). In contrast, TRIM25 expression did not induce the ubiquitination of GST–MDA5(2CARD) (Supplementary Fig. 4b). TRIM25 depletion *in vivo* by a TRIM25-specific small hairpin RNA (shRNA)[13] significantly reduced the ubiquitination level of GST–RIG-I(2CARD) and RIG-I in a dose-dependent manner (Fig. 3c and Supplementary Fig. 5a), but a nonspecific scrambled-sequence shRNA had no effect on GST–RIG-I(2CARD) ubiquitination (Supplementary Fig. 5b). Finally, an *in vitro* ubiquitination assay showed that TRIM25 effectively delivered the ubiquitin moieties to maltose-binding protein (MBP)–T7-tagged RIG-I(2CARD), but not MBP–T7 alone or MBP–T7–RIG-I(2CARD(170stop)) (Fig. 3d and Supplementary Fig. 6a). Consistent with its ubiquitination level, RIG-I-mediated induction of IFN-β or NF-κB promoter activity considerably increased on TRIM25 expression in a dose-dependent manner (Fig. 3e and Supplementary Fig. 6b). Notably, expression of the TRIM25(SPRY) mutant, which was sufficient to bind to RIG-I, markedly suppressed GST–RIG-I(2CARD) ubiquitination in a dose-dependent manner (Fig. 3f) as well as endogenous RIG-I ubiquitination (Supplementary Fig. 4a). Furthermore, expression of the TRIM25(SPRY) mutant considerably decreased the RIG-I 2CARD-mediated activation of IFN-β or NF-κB promoter activity in a dose-dependent manner (Supplementary Fig. 7). This suggests that TRIM25-mediated ubiquitination has an important role in RIG-I signalling activity.

Unlike the GST–RIG-I(2CARD) K172R mutant, which showed an almost complete loss of ubiquitination and IFN-β and NF-κB promoter activation, GST–RIG-I(2CARD) K172only—containing five K→R substitutions but leaving K172 intact—demonstrated highly induced IFN-β and NF-κB promoter activity (Fig. 4a, b). Furthermore, the GST–RIG-I(2CARD) K172only mutant underwent robust ubiquitination (albeit lower than that of wild-type GST–RIG-I(2CARD)) on TRIM25 expression, whereas GST–RIG-I(2CARD) K172R was minimally ubiquitinated (Fig. 4c). However, despite a significant reduction in its level of ubiquitination, GST–RIG-I(2CARD) K172R interacted with TRIM25 as efficiently as wild-type GST–RIG-I(2CARD) and the K172only mutant (Fig. 4c). As seen with RIG-I(2CARD), full-length RIG-I K172only but not RIG-I K172R demonstrated ubiquitination at the same level as RIG-I wild type (Supplementary Fig. 8). Finally, correlated with their ubiquitination levels, expression of wild-type RIG-I and mutant RIG-I K172only in *RIG-I*$^{-/-}$ mouse embryonic fibroblasts (MEFs) induced IFN-β production on Sendai virus infection, whereas expression of mutant RIG-I K172R showed no effect on IFN-β production (Supplementary Fig. 9).

The 2CARD of RIG-I has been shown to bind to the MAVS CARD to elicit downstream signal transduction[14–17]. GST pull-down analysis showed that wild-type GST–RIG-I(2CARD) and mutant GST–RIG-I(2CARD) K172only efficiently interacted with the Flag-tagged CARD proline-rich domain of MAVS (Flag–MAVS(CARD-PRD)), whereas GST–RIG-I(2CARD) K172R and GST–RIG-I(2CARD) K99,169,172, 181,190,193R mutants poorly bound to Flag–MAVS(CARD-PRD) (Fig. 4d), indicating that Lys 172 is critical for TRIM25-mediated ubiquitination, RIG-I signalling and MAVS interaction, but not for TRIM25 binding (Fig. 4c).

Wild-type, *Trim25*$^{+/-}$ and *Trim25*$^{-/-}$ MEFs[18] were used to test the direct contribution of TRIM25 to RIG-I-mediated IFN-β expression. IFN-β promoter activity was very low in *Trim25*$^{-/-}$ MEFs and was reduced in *Trim25*$^{+/-}$ MEFs compared with wild-type MEFs

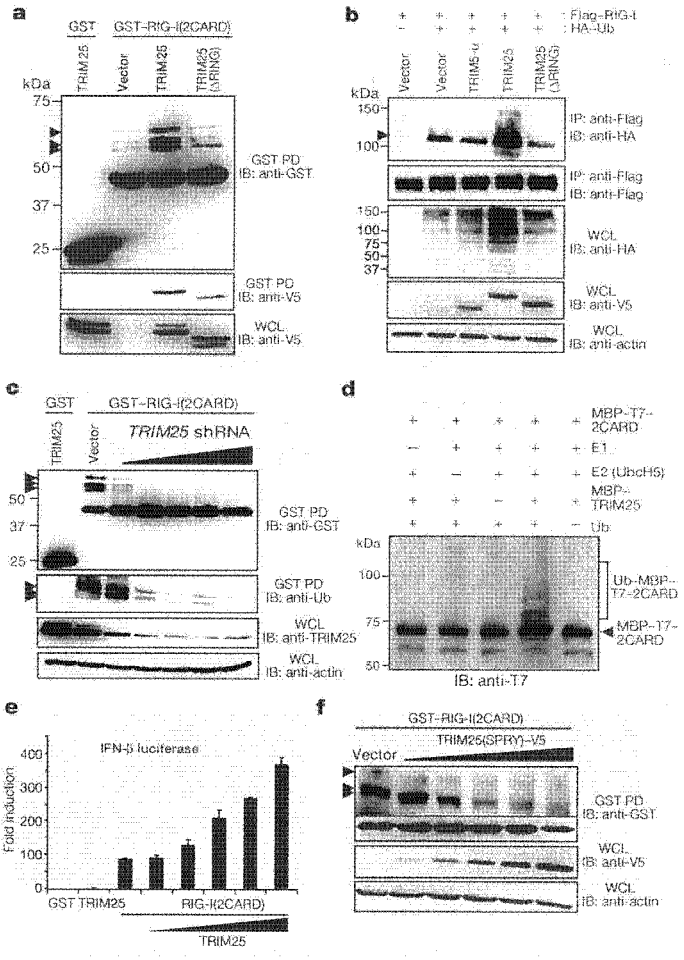

Figure 3 | TRIM25 is a primary E3 ubiquitin ligase of RIG-I. HEK293T cells transfected with GST or GST–RIG-I(2CARD) (**a**) or Flag–RIG-I and HA–ubiquitin (**b**) together with vector, TRIM25, TRIM25(ΔRING) or TRIM5-α were used for GST pull down (PD) (**a**) or immunoprecipitation with anti-Flag antibody (**b**). **c**, HEK293T cells transfected with GST or GST–RIG-I(2CARD) together with pSUPER.retro.puro or *TRIM25*-shRNA-specific pSUPER.retro.puro[13] were used for GST pull down. Arrows indicate the ubiquitinated GST–RIG-I(2CARD) and Flag–RIG-I. **d**, *In vitro* ubiquitination was detected by anti-T7 immunoblotting. **e**, IFN-β luciferase activity in HEK293T cells transfected with GST–RIG-I(2CARD) and TRIM25. The results are expressed as means ± s.d. ($n = 3$). **f**, HEK293T cells transfected with GST–RIG-I(2CARD) and V5–TRIM25(SPRY) were used for GST pull down. Arrows indicate ubiquitinated GST–RIG-I(2CARD).

(Supplementary Fig. 10a). Consistent with IFN-β promoter activation, virus-induced IFN-β production was virtually undetectable in *Trim25*$^{-/-}$ MEFs, whereas it was considerably high in wild-type MEFs (Fig. 4e). *Trim25*$^{+/-}$ MEFs showed a slightly reduced level of IFN-β production compared with wild-type MEFs (Fig. 4e). On vesicular stomatitis virus (VSV)–enhanced green fluorescent protein (eGFP) infection at various multiplicity of infections (MOIs), *Trim25*$^{-/-}$ MEFs showed remarkably increased levels of VSV–eGFP-positive cells (Fig. 4g and Supplementary Fig. 10b) and increased VSV yields (over 100-fold) (Fig. 4f) compared with wild-type and *Trim25*$^{+/-}$ MEFs. Similarly, *Trim25*$^{-/-}$ MEFs showed a considerable increase in the level of Newcastle disease virus (NDV)–GFP infection (Supplementary Fig. 10c). Finally, TRIM25 expression significantly suppressed VSV–eGFP replication in HEK293T cells, whereas expression of the TRIM25(SPRY) mutant detectably increased VSV–eGFP replication (Fig. 4h). Collectively, these results indicate that TRIM25 is critical for cytosolic RIG-I signal transduction that mediates the induction of the IFN response on viral infection.

Ubiquitination is a versatile post-translational modification involved in various cellular functions[19]. Our study indicates that TRIM25 E3 ubiquitin ligase induces the Lys 63-linked ubiquitination of RIG-I; that Lys 172 is the critical site for TRIM25-mediated ubiquitination; and that, as seen with the ubiquitin-dependent interaction between RIP and NEMO[20], the TRIM25-mediated ubiquitination of RIG-I may facilitate its interaction with MAVS, which ultimately leads to downstream signal transduction. Thus, the interconnection between the RIG-I cytosolic viral RNA receptor and a member of the TRIM family represents a new class of antiviral regulatory pathway involved in innate immunity.

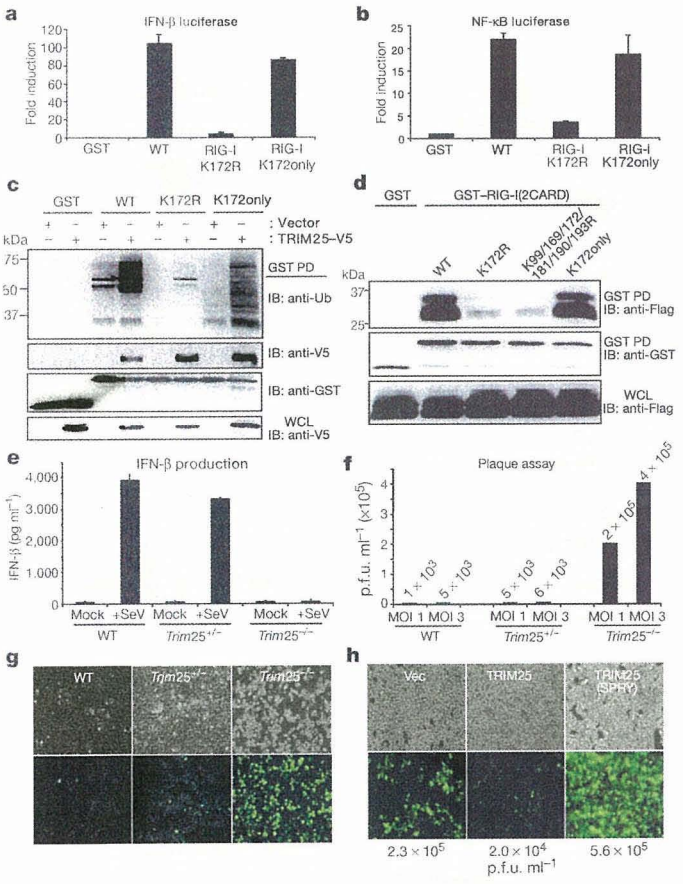

Figure 4 | Role of TRIM25-mediated ubiquitination in RIG-I antiviral activity. IFN-β (**a**) and NF-κB (**b**) promoter activity in GST–RIG-I(2CARD) or mutant transfected cells. The results are expressed as means ± s.d. ($n = 3$). **c**, HEK293T cells transfected with GST–RIG-I(2CARD), GST–RIG-I(2CARD) K172R, or GST–RIG-I(2CARD) K172only together with vector or TRIM25 were used for GST pull down. **d**, HEK293T cells transfected with GST–RIG-I(2CARD) or the indicated mutants together with Flag–MAVS(CARD-PRD) were used for GST pull down. **e**, IFN-β production in wild-type, *Trim25*$^{+/-}$ and *Trim25*$^{-/-}$ MEFs upon Sendai virus infection. The results are expressed as means ± s.d. ($n = 3$). **f–h**, VSV–eGFP replication in wild-type, *Trim25*$^{+/-}$ and *Trim25*$^{-/-}$ MEFs (**f** and **g**) or in vector-, TRIM25-, or TRIM25(SPRY)-expressing HEK293T cells (**h**) was determined by plaque assay or visualized by fluorescence microscopy.

METHODS SUMMARY

RNA interference for TRIM25. The mammalian expression vector pSUPER.retro.puro (OligoEngine), encoding shRNAs for *TRIM25* sequence, was provided by D.-E. Zhang. Details of the shRNA sequence and transfection method have been described[13].

Viruses. NDV–GFP and VSV–eGFP were provided by A. Garcia-Sastre and S. Whelan, respectively.

Measurement of IFN-β production. Cell culture supernatants were collected and analysed for IFN-β production using enzyme-linked immunosorbent assays (PBL Biomedical Laboratories).

***In vitro* ubiquitination assay.** Purified MBP–T7–RIG-I(2CARD) (20 μg ml^{-1}) and MBP–TRIM25 (20 μg ml^{-1}) derived from *Escherichia coli* were incubated in a reaction buffer (50 mM Tris-HCl, 2 mM dithiothreitol, 5 mM $MgCl_2$ and 4 mM ATP) with ubiquitin (50 μg ml^{-1}; Sigma), human recombinant E1 (1.6 μg ml^{-1}; BIOMOL) and human recombinant UbcH5a (20 μg ml^{-1}; BIOMOL) at 32 °C for 2 h and subjected to immunoblotting with anti-T7 antibody (Novagen).

Full Methods and any associated references are available in the online version of the paper at www.nature.com/nature.

Received 14 February; accepted 8 March 2007.
Published online 28 March 2007.

1. Honda, K., Takaoka, A. & Taniguchi, T. Type I interferon gene induction by the interferon regulatory factor family of transcription factors. *Immunity* 25, 349–360 (2006); erratum 25, 849 (2006).
2. Hornung, V. *et al.* 5′-Triphosphate RNA is the ligand for RIG-I. *Science* 314, 994–997 (2006).
3. Meylan, E. & Tschopp, J. Toll-like receptors and RNA helicases: two parallel ways to trigger antiviral responses. *Mol. Cell* 22, 561–569 (2006).
4. Pichlmair, A. *et al.* RIG-I-mediated antiviral responses to single-stranded RNA bearing 5′-phosphates. *Science* 314, 997–1001 (2006).
5. Stetson, D. B. & Medzhitov, R. Antiviral defense: interferons and beyond. *J. Exp. Med.* 203, 1837–1841 (2006).
6. Yoneyama, M. *et al.* The RNA helicase RIG-I has an essential function in double-stranded RNA-induced innate antiviral responses. *Nature Immunol.* 5, 730–737 (2004).
7. Nisole, S., Stoye, J. P. & Saib, A. TRIM family proteins: retroviral restriction and antiviral defence. *Nature Rev. Microbiol.* 3, 799–808 (2005).
8. Johnson, C. L. & Gale, M. Jr. CARD games between virus and host get a new player. *Trends Immunol.* 27, 1–4 (2006).
9. Meylan, E., Tschopp, J. & Karin, M. Intracellular pattern recognition receptors in the host response. *Nature* 442, 39–44 (2006).
10. Kato, H. *et al.* Cell type-specific involvement of RIG-I in antiviral response. *Immunity* 23, 19–28 (2005).
11. Orimo, A., Inoue, S., Ikeda, K., Noji, S. & Muramatsu, M. Molecular cloning, structure, and expression of mouse estrogen-responsive finger protein Efp. Co-localization with estrogen receptor mRNA in target organs. *J. Biol. Chem.* 270, 24406–24413 (1995).
12. Urano, T. *et al.* Efp targets 14-3-3σ for proteolysis and promotes breast tumour growth. *Nature* 417, 871–875 (2002).
13. Zou, W. & Zhang, D. E. The interferon-inducible ubiquitin-protein isopeptide ligase (E3) EFP also functions as an ISG15 E3 ligase. *J. Biol. Chem.* 281, 3989–3994 (2006).
14. Meylan, E. *et al.* Cardif is an adaptor protein in the RIG-I antiviral pathway and is targeted by hepatitis C virus. *Nature* 437, 1167–1172 (2005).
15. Seth, R. B., Sun, L., Ea, C. K. & Chen, Z. J. Identification and characterization of MAVS, a mitochondrial antiviral signaling protein that activates NF-κB and IRF 3. *Cell* 122, 669–682 (2005).
16. Xu, L. G. *et al.* VISA is an adapter protein required for virus-triggered IFN-β signaling. *Mol. Cell* 19, 727–740 (2005).
17. Kawai, T. *et al.* IPS-1, an adaptor triggering RIG-I- and Mda5-mediated type I interferon induction. *Nature Immunol.* 6, 981–988 (2005).
18. Orimo, A. *et al.* Underdeveloped uterus and reduced estrogen responsiveness in mice with disruption of the estrogen-responsive finger protein gene, which is a direct target of estrogen receptor α. *Proc. Natl Acad. Sci. USA* 96, 12027–12032 (1999).

19. Haglund, K. & Dikic, I. Ubiquitylation and cell signaling. *EMBO J.* **24**, 3353–3359 (2005).
20. Ea, C. K., Deng, L., Xia, Z. P., Pineda, G. & Chen, Z. J. Activation of IKK by TNFα requires site-specific ubiquitination of RIP1 and polyubiquitin binding by NEMO. *Mol. Cell* **22**, 245–257 (2006).
21. Kirkpatrick, D. S., Denison, C. & Gygi, S. P. Weighing in on ubiquitin: the expanding role of mass-spectrometry-based proteomics. *Nature Cell Biol.* **7**, 750–757 (2005).

Supplementary Information is linked to the online version of the paper at www.nature.com/nature.

Acknowledgements This work was supported by US Public Health Service grants (J.U.J.), the exchange programme between Harvard Medical School and the graduate training programme 1071 at the Friedrich-Alexander University Erlangen-Nuremberg, Germany (M.U.G.), and a Korea Research Foundation Grant (C.-H.J.). We thank A. Garcia-Sastre, D.-E. Zhang and S. Whelan for providing reagents, and R. Tomaino and J. Nagel for mass spectrometry. We also thank all members of the Tumor Virology Division, New England Primate Research Center, for discussions.

Author Contributions M.U.G. performed all aspects of this study. Y.C.S., C.-H.J. and C.L. assisted in experimental design and in collecting the data. T.U. and S.I. performed the *in vitro* ubiquitination assay and generated *Trim25*$^{-/-}$ MEFs. L.S. and Z.C. generated the MAVS construct and RIG-I antibody. T.O. and S.A. generated the RIG-I construct and *RIG-I*$^{-/-}$ MEFs. M.U.G. and J.U.J. organized this study and wrote the paper. All authors discussed the results and commented on the manuscript.

Author Information Reprints and permissions information is available at www.nature.com/reprints. The authors declare no competing financial interests. Correspondence and requests for materials should be addressed to J.U.J. (jae_jung@hms.harvard.edu).

METHODS

Cell culture. HEK293T, MEF and Hela cells were cultured in Dulbecco's modified Eagle's medium supplemented with 10% fetal bovine serum, 2 mM L-glutamine and 1% penicillin-streptomycin (Gibco-BRL). Transient transfections were performed with FuGENE 6 (Roche), lipofectamine 2000 (Invitrogen), or calcium phosphate (Clontech) following the manufacturer's instructions. Wild-type, *Trim25*$^{+/-}$ and *Trim25*$^{-/-}$ MEFs were immortalized with LXSN-E6/E7 retroviral vector containing human papilloma virus 16 E6 and E7 oncogenes using a standard protocol of selection with 200 μg ml^{-1} of neomycin. *RIG-I*$^{-/-}$ MEFs were infected with pBabe-puro vector, pBabe-puro-RIG-I wild-type, pBabe-puro-RIG-I K172R, or pBabe-puro-RIG-I K172only retrovirus, followed by selection with 1 μg ml^{-1} of puromycin.

Plasmid construction. All constructs for transient and stable expression in mammalian cells were derived from the pEBG GST fusion vector and the pEF-IRES-Puro expression vector. DNA fragments corresponding to the coding sequence of the *RIG-I* and *TRIM25* genes were amplified from template DNA by polymerase chain reaction (PCR) and subcloned into plasmid pEBG between restriction sites *Kpn*I and *Not*I or pEF-IRES-puro between *Afl*II and *Not*I for selection of stable transfectants. V5-tagged TRIM25 and Flag-tagged RIG-I were expressed from a modified pIRES-puro encoding a C-terminal V5 tag and Flag tag, respectively. RIG-I mutants were generated by PCR using site-directed mutagenesis. All constructs were sequenced using an ABI PRISM 377 automatic DNA sequencer to verify 100% agreement with the original sequence.

***In vivo* GST pull down, protein purification and mass spectrometry.** At 48 h after transfection with vectors expressing GST, GST–RIG-I(2CARD) or GST–MDA5(2CARD) fusions, HEK293T cells were collected and lysed with NP40 buffer (50 mM HEPES, pH 7.4, 150 mM NaCl, 1 mM EDTA, 1% (v/v) NP40) supplemented with a complete protease inhibitor cocktail (Roche). Post-centrifuged supernatants were pre-cleared with protein A/G beads at 4 °C for 2 h. Pre-cleared lysates were mixed with a 50% slurry of glutathione-conjugated Sepharose beads (Amersham Biosciences), and the binding reaction was incubated for 4 h at 4 °C. Precipitates were washed extensively with lysis buffer. Proteins bound to glutathione beads were eluted and separated on a NuPAGE 4–12% Bis-Tris gradient gel (Invitrogen). After Coomassie or silver staining (Invitrogen), specific protein bands were excised and analysed by ion-trap mass spectrometry at the Harvard Taplin Biological Mass Spectrometry facility, and amino acid sequences were determined by tandem mass spectrometry and database searches.

Immunoblot analysis and immunoprecipitation assay. For immunoblotting, polypeptides were resolved by SDS–polyacrylamide gel electrophoresis (SDS–PAGE) and transferred to a PVDF membrane (Bio-Rad). Immunodetection was achieved with anti-V5 (1:5,000) (Invitrogen), anti-Flag (1:5,000) (Sigma), anti-HA (1:5,000), anti-GST (1:10,000) (Sigma), anti-actin (1:10,000) (Abcam), or anti-TRIM25 (1:2,000) (BD Bioscience) antibodies. The proteins were visualized by a chemiluminescence reagent (Pierce) and detected by a Fuji Phosphor Imager.

For immunoprecipitation, cells were collected after 48 h and then lysed in NP40 buffer supplemented with a complete protease inhibitor cocktail (Roche). After pre-clearing with protein A/G agarose beads for 2 h at 4 °C, whole-cell lysates were used for immunoprecipitation with the indicated antibodies. Generally, 1–2 μg of commercial antibody was added to 1 ml of cell lysate, which was incubated at 4 °C for 4–12 h. After addition of protein A/G agarose beads, the incubation was continued for 2 h. Immunoprecipitates were extensively washed with lysis buffer and eluted with SDS loading buffer by boiling for 5 min.

Confocal immunofluorescence microscopy. Eighteen to twenty-four hours after transfection, cells were fixed with 4% paraformaldehyde for 15 min, permeabilized with 0.2% (v/v) Triton X-100 for 15 min, blocked with 10% goat serum in PBS for 1 h and reacted with diluted primary antibody in 1% goat serum for up to 2 h at room temperature. After incubation, cells were washed extensively with PBS, incubated with the appropriate secondary antibody diluted in 1% goat serum for 1 h at room temperature, and washed three times with PBS. Confocal microscopy was performed using a Leica TCS SP laser-scanning microscope (Leica Microsystems) fitted with a ×100 Leica objective (PL APO, 1.4NA) and Leica imaging software. Images were collected at 512 × 512-pixel resolution. The stained cells were optically sectioned in the *z* axis, and the images in the different channels (photo multiplier tubes) were collected simultaneously. The step size in the *z* axis varied from 0.2 to 0.5 μm to obtain 16 slices per imaged file. The images were transferred to a Macintosh G4 computer (Apple Computer), and Photoshop (Adobe) was used to render the images.